ACS APPLIED MATERIALS & INTERFACES

Research Article

www.acsami.org

Control of Interfacial Layers for High-Performance Porous Si Lithium-Ion Battery Anode

Hyungmin Park, Sungjun Lee, Seungmin Yoo, Myoungsoo Shin, Jieun Kim, Myungjin Chun, Nam-Soon Choi,* and Soojin Park*

School of Energy and Chemical Engineering, Department of Energy Engineering, Ulsan National Institute of Science and Technology (UNIST), UNIST-gil 50, Ulsan 689-798, Republic of Korea

Supporting Information

ABSTRACT: We demonstrate a facile synthesis of micrometer-sized porous Si particles via copper-assisted chemical etching process. Subsequently, metal and/or metal silicide layers are introduced on the surface of porous Si particles using a simple chemical reduction process. Macroporous Si and metal/metal silicide-coated Si electrodes exhibit a high initial Coulombic efficiency of ~90%. Reversible capacity of carbon-coated porous Si gradually decays after 80 cycles, while metal/metal silicide-coated porous Si electrodes show significantly improved cycling performance even after 100 cycles with a reversible capacity of >1500 mAh g^{-1}. We confirm that a stable solid-electrolyte interface layer is formed on metal/metal silicide-coated porous Si electrodes during cycling, leading to a highly stable cycling performance.

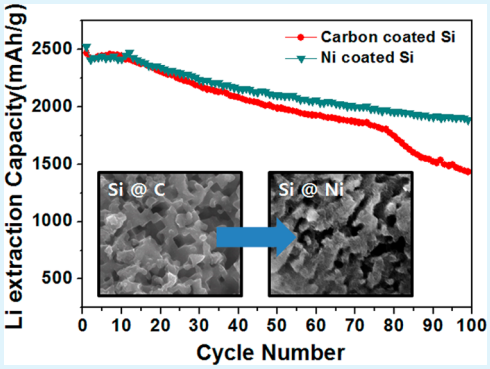

KEYWORDS: *lithium-ion batteries, porous Si anode, interfacial coating layer, solid electrolyte interphase, surface coating*

INTRODUCTION

As there is increased demand of energy from mobile electronic devices to large-scale energy storage systems, lithium-ion batteries (LIBs) have been given much attention due to their high power and high energy density. Carbonaceous materials (e.g., natural graphite, mesophase carbon microbeads, and carbon nanofiber) have been used as the anode material in commercialized LIBs. However, limited capacity (>350 mAh g^{-1}) of the carbon-based anode materials is urging development of alternative materials with a high specific capacity. Lithium alloying materials (e.g., Si, Ge, Sn, Sb, etc.) and metal oxides (CuO, SnO_2, NiO, etc.) with various morphologies have been developed.[1−8]

Among them, silicon (Si) is a promising anode material, because it is abundant, is cheap, has a low working potential (<0.5 V vs Li/Li^+), and has a high theoretical capacity (3579 mAh g^{-1} for $Li_{15}Si_4$). However, Si electrodes suffer from a large volume change (>300%) during the lithiation/delithiation process, resulting in poor cycling life due to pulverization and subsequent loss of electrical contact between the active material and the current collector.[9,10]

To solve this problem, numerous nanostructured Si structures were proposed to sustain their own structures such as thin film,[11−14] nanoparticles,[15,16] York−shell,[17−19] nanowires,[20] and nanotubes.[21,22] These nanostructured Si electrodes showed significantly improved electrochemical performances, including a high specific capacity, long-term cycling stability, and improved rate capabilities.[11−22] However, nanostructuring of nanosized Si particles has several disadvantages in practical LIB applications due to high production cost, complicated synthetic route, and low packing density.[23,24]

A plausible strategy is to introduce a nanostructuring concept in micrometer-sized Si particles by using several methods, like metal-assisted chemical etching, catalytic growth of nanowires onto the Si surface, and microassembly of nanoparticles.[25−27] Another problem of Si is an intrinsically low electrical conductivity (band gap of ~1.2 eV in bulk Si). To enhance the electrical conductivity of Si particles, various coating layers such as carbon,[28−30] metal,[31,32] metal oxide,[33] conducting polymers,[34] and metal silicide[15,35] have been introduced on the Si surface. Among them, metal silicide-coated Si electrode showed superior electrochemical performances due to a formation of stable solid-electrolyte interface (SEI) layer and increased electrical conductivity.[15,35] However, the effect of various metal silicide coating layers on the electrochemical properties of Si-based electrodes was not clearly described in other reports.

Herein, we demonstrate a facile synthesis of micrometer-sized porous Si particles via copper-assisted wet chemical etching and subsequent introduction of electrically conductive metal and/or metal silicide layers on the Si surface. Our investigation reveals that porous Si and metal/metal silicide-coated Si anodes exhibit remarkably high initial Coulombic efficiency of ~90%. Reversible capacity of bare porous Si

Received: July 16, 2014
Accepted: August 25, 2014
Published: August 25, 2014

   dx.doi.org/10.1021/am5046197 | ACS Appl. Mater. Interfaces 2014, 6, 16360−16367

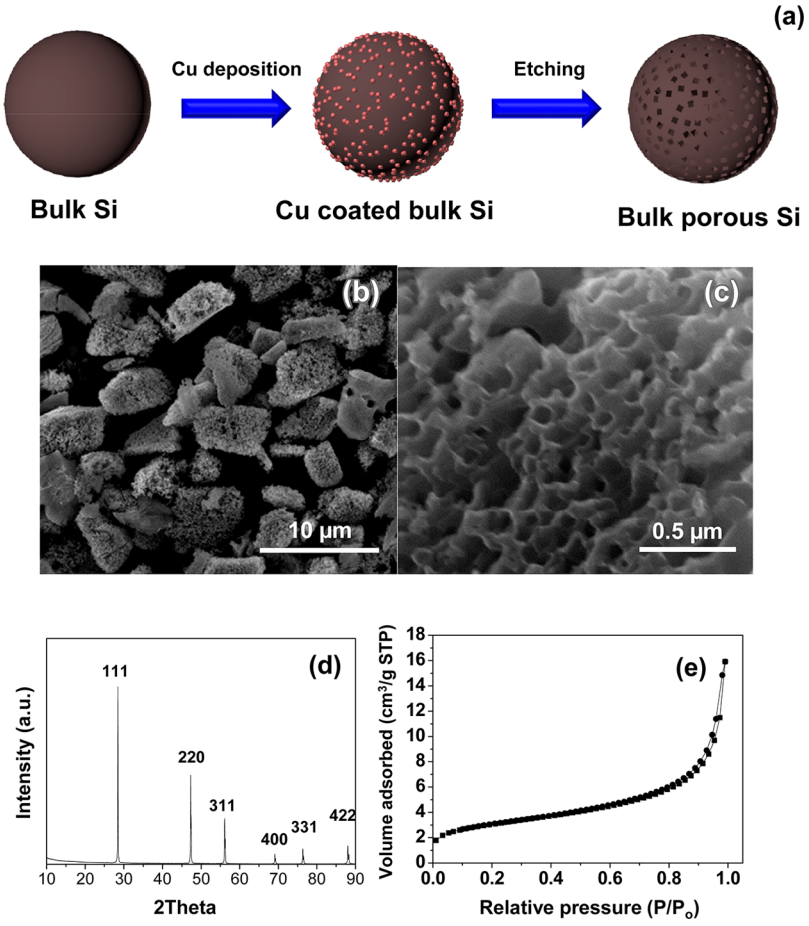

Figure 1. (a) Schematic illustration showing the synthetic route of porous Si particles via Cu-assisted chemical etching. (b) Low-magnified and (c) high-magnified SEM images of as-synthesized macroporous Si particles. (d) XRD pattern of as-synthesized porous Si particles. (e) Nitrogen adsorption/desorption isotherm of porous Si powder.

dramatically decreases after 60 cycles at C/5 rate, while carbon-coated porous Si gradually decays after 80 cycles at the same rate. In contrast, metal/metal silicide-coated porous Si electrodes show significantly improved cycling performance even after 100 cycles with a reversible capacity of >1500 mAh g^{-1}. We confirm that metal/metal silicide-coated Si forms a stable SEI layer on the Si surface during cycling, leading to a highly stable cycling performance.

EXPERIMENTAL SECTION

Synthesis of Macroporous Si Particles. To synthesize micrometer-sized macroporous Si, Si powders (particle size of ~10 μm, Shandong Co., China), copper sulfate ($CuSO_4$, Sigma-Aldrich), hydrofluoric acid (HF, J.T. Baker), and hydrogen peroxide (H_2O_2, Samchun, Korea) were purchased. In a typical metal-assisted chemical etching process, 50 g of Si particles was added to a solution of 40 mM $CuSO_4$ and 5 M HF with stirring at 50 °C for 12 h to make porous Si structures. Subsequently, the remaining Cu particles were completely dissolved in concentrated nitric acid at 50 °C for 3 h.

Carbon-Coated Porous Si Particles. Porous Si particles (1 g) were exposed to toluene vapor with argon purging at 900 °C (with a heating rate of 10 °C/min) in a quartz tube furnace. At this temperature, toluene vapor was transformed to amorphous carbon. The carbon contents were controlled with exposure time of toluene vapor. In this study, carbon of 10 wt % was deposited on the Si surface at 900 °C for 10 min in a stream of argon/toluene.

Cu/Cu_3Si-Coated Si Particles. 10 mL of 0.1 M aqueous $Cu(NO_3)_2 \cdot 2.5H_2O$ (Sigma-Aldrich) solution and 20 mL of 0.1 M aqueous LiOH (Sigma-Aldrich) were mixed together and heated up to 70 °C. Porous Si powder (1 g) was added into the mixture with vigorous stirring. Then 0.1 mL N_2H_4 solution (35 wt %, Sigma-Aldrich) was added to the mixed solution. After 10 min, the final product was rinsed with deionized water and dried completely in a vacuum oven. The dried powder was annealed at 750 °C for 1 h in argon atmosphere to make Cu/Cu_3Si-coated Si particles.

Ni-Coated Si Particles. 10 mL of 0.1 M aqueous $NiCl_2$ (Sigma-Aldrich) solution and 1.5 mL of NH_4OH solution (Sigma-Aldrich) were mixed together at room temperature with vigorous stirring and heated to 80 °C. Subsequently, 1 g of porous Si particles was added to this mixture to make $Ni(OH)_2$-coated Si particles. In the final step, $Ni(OH)_2$-coated Si particles were converted to Ni-coated Si by thermal annealing at 300 °C for 1 h in Ar/H_2 forming gas.

Fe_2Si-Coated Si Particles. 5 mL of 0.1 M aqueous $Fe(NO_3)_3 \cdot 9H_2O$ (Sigma-Aldrich) solution were mixed with 1 g of porous Si powder at 60 °C with vigorous stirring. At this temperature, water is slowly evaporated to make a uniform mixture of Fe/Si. Subsequent thermal annealing at 900 °C for 1 h in Ar/H_2 (96/4) forming gas led to a formation of $FeSi_2$-coated Si particles.

Characterization. Scanning electron microscopy (Nano SEM 230, FEI) was used to characterize porous Si, Si particles with various coating layers at an accelerating voltage of 10 kV. A cross-sectional view of each electrode of pristine and after 100 cycles was observed after disassembling cells in the glovebox. The nitrogen adsorption and desorption isotherms were measured with a VELSORP-mini (BEL Japan, Inc.) at 77 K in the relative pressure range of P/P_0 from 0.05 to 0.3 to obtain the Brunauer–Emmett–Teller (BET) surface areas. X-ray diffraction (D8 ADVANCE, Bruker) was used to investigate microstructures of Si and metal/metal silicide-coating layers. To characterize solid-electrolyte interface layers of Si electrodes, X-ray

dx.doi.org/10.1021/am5046197 | ACS Appl. Mater. Interfaces 2014, 6, 16360–16367

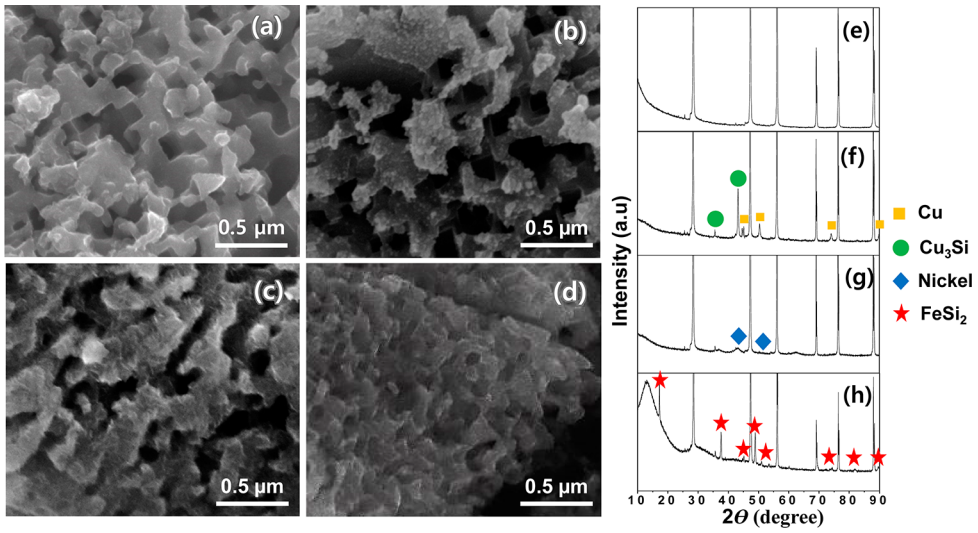

Figure 2. Porous Si particles with various coating layers. SEM images of macroporous Si particles coated with (a) carbon, (b) Cu/Cu_3Si, (c) Ni, and (d) $FeSi_2$ layers. XRD patterns of macroporous Si particles coated with (e) carbon, (f) Cu/Cu_3Si, (g) Ni, and (h) $FeSi_2$ layers.

photoelectron spectroscopy (XPS) was used. Impedance analysis was performed on IVIUM frequency response analyzer ranging from 0.01 Hz to 100 kHz.

Electrochemical Test. The coin cell was assembled to evaluate electrochemical properties of Si-based electrodes. The Si electrodes were prepared by spreading a slurry mixture of porous Si powder, poly(acrylic acid) (PAA, weight-average molecular weight = 100 kg/mol, Aldrich), sodium carboxymethyl cellulose (CMC, 4 wt % in H_2O, Aldrich), and super P (70:20:10 in weight ratio) on a piece of Cu foil. Specifically, the slurry was mixed with a mixer (Thinky mixer, ARE310) at a high speed (2200 rpm) to homogenize for 10 min. After spreading the slurry mixture, electrodes were dried at 150 °C for 60 min in a vacuum oven. The area loading level of all electrodes was 3−4 mAh/cm^2. Galvanostatic charge and discharge cycling (WonATech WBCS 3000 battery measurement system) was performed in the potential window from 0.005 to 1.2 V (versus Li/Li^+) with a 2016 coin-type half-cell. The electrolyte comprised 1.3 M $LiPF_6$ in a mixture of ethylene carbonate (EC) and diethyl carbonate (DEC) (30:70, v/v) with additive of 10% fluorinated ethylene carbonate (FEC). Microporous polyethylene film (Celgard 2400) was used as a separator. Cells were assembled in an Ar-filled glovebox with <1 ppm of both oxygen and moisture. After cycling, cells were carefully opened in a glovebox to retrieve their electrodes, and electrodes were subsequently rinsed in dimethyl carbonate (DMC) to remove a residual $LiPF_6$-based electrolyte and then dried at room temperature. To confirm the cross-sectional view, dried electrodes were immerged in liquid nitrogen for 10 s. Then the electrodes were cut with scissors quickly to obtain cross-sectioned electrodes.

RESULTS AND DISCUSSION

Synthesis of Macroporous Si Particles with Various Coating Layers. Figure 1a shows a schematic illustration showing the synthetic process of micrometer-sized porous Si particles via copper-assisted chemical etching process. For a typical Cu-assisted chemical etching process, 50 g of Si particles (an average particle size of 10 μm) were added to a solution of 40 mM copper sulfate and 5 M hydrofluoric acid (HF) with stirring at 50 °C for 12 h to make porous Si structures. Subsequently, the remaining Cu particles were completely dissolved in concentrated nitric acid at 50 °C for 3 h. Figure 1b shows a scanning electron microscopy (SEM) image of chemically etched porous Si particles with a particle size of 3−5 μm. From the magnified SEM image, macropores of 100−200 nm are clearly seen (Figure 1c). The X-ray diffraction (XRD) pattern of porous Si particles indicates that pure crystalline Si is obtained after chemical etching without any other impurities (Figure 1d). We investigated the surface area of the porous Si particles by nitrogen adsorption/desorption experiment. From a Brunauer−Emmett−Teller (BET) isotherm plot, the surface area of the porous Si particles is 7.12 m^2/g, indicating that macropores are formed in the Si particles (Figure 1e).

Since Si materials have intrinsically low electrical conductivity, various conductive materials (e.g., carbon, conductive polymers, metals, and metal silicides) have been introduced on the Si surface.[15,28−35] First, we used the conventional carbon-coating process, in which toluene vapor as a carbon source was introduced to Si particles and subsequently carbonized at 900 °C for 30 min to obtain carbon-coated Si particles. Carbon contents of ∼10 wt % were measured by inductively coupled plasma mass spectrometry (ICP). An SEM image of carbon-coated Si particles shows that pore size of as-synthesized porous Si particles decreases; however, the original porous structure of Si particles was not destroyed after the carbon-coating process, as shown in Figure 2a. Also, the XRD pattern of carbon-coated Si particles shows only crystalline Si peaks, indicating that amorphous carbon layers are coated on the Si surface (Figure 2e). Furthermore, amorphous characteristics of carbon layers were confirmed by Raman spectrum (Supporting Information, Figure S1).

Second, the Cu/Cu_3Si-coating process was conducted by a simple chemical reduction process. Copper nitrate ($Cu(NO_3)_2$) and lithium hydroxide (LiOH) were mixed together at 70 °C to make copper hydroxide ($Cu(OH)_2$)-coated Si particles. Subsequently, addition of reducing agents (hydrazine, N_2H_4) to the solution led to a formation of Cu-coated Si particles. Cu nanoparticles with diameter of 20−30 nm are uniformly coated on the surface of Si particles with Cu contents of ∼10 wt % as confirmed by ICP analysis (Figure 2b). Subsequently, the thermal annealing process was applied to Cu-coated Si particles at 750 °C for 1 h in argon atmosphere to make Cu/Cu_3Si-coated Si particles, as confirmed by XRD patterns (Figure 2f). Previously, Kim et al. reported that alloying reaction between Si and Cu occurs at ∼300 °C.[36] However, in our case, small amounts of Cu particles did not react with Si. Probably the size

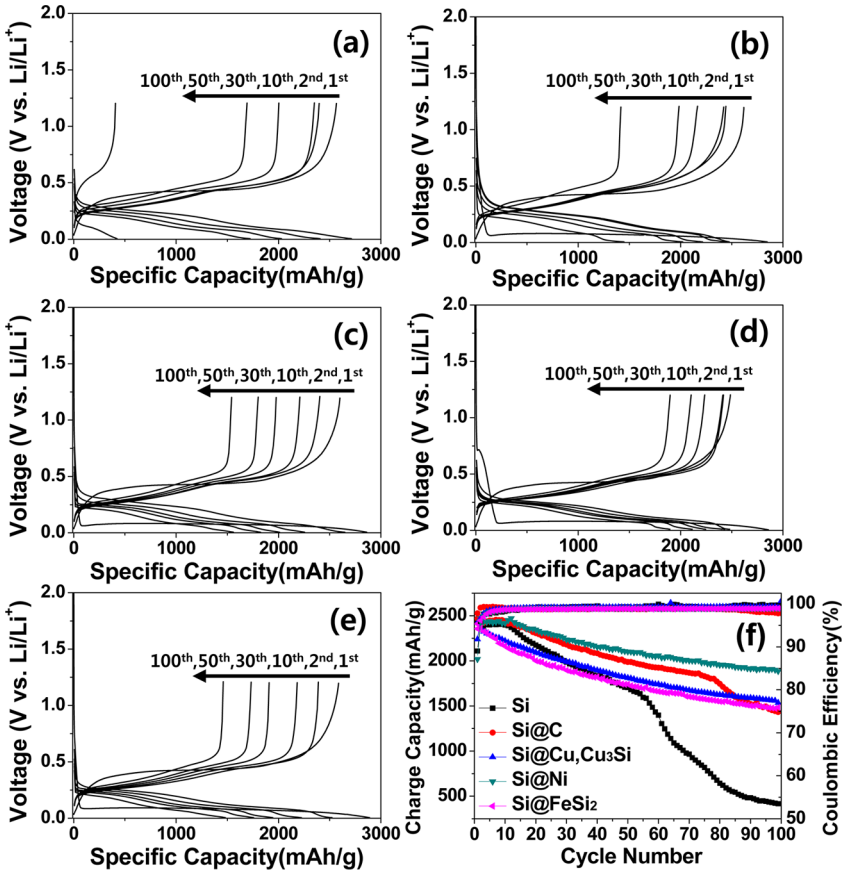

Figure 3. Electrochemical properties of porous Si electrodes with various coating layers. Voltage profiles of (a) porous Si, (b) carbon-coated Si, (c) Cu/Cu_3Si-coated Si, (d) Ni-coated Si, and (e) $FeSi_2$-coated Si electrodes obtained at a rate of C/20 (first cycle) and C/5 (subsequent cycles) in the range of 0.005−1.2 V. (f) Cycling performance and Coulombic efficiency of five different Si-based electrodes at C/5 discharging−charging.

of the Cu particle and the annealing condition play a key role in synthesizing pure copper silicide.

Third, we synthesized Ni-coated Si particles. An aqueous nickel chloride ($NiCl_2$) and ammonium hydroxide (NH_4OH) mixture was prepared at 80 °C, and this was followed by addition of Si particles with vigorous stirring to make flake-type $Ni(OH)_2$-coated Si particles. Subsequent thermal annealing at 300 °C in Ar/H_2 (95/5) led to a formation of Ni-coated Si particles (Figure 2c and g). Typically, nickel silicide layers are formed at the interface between Si and Ni after thermal annealing at >300 °C in Ar/H_2 environment.[37] However, flake-type Ni sheets prepared in this study are not fully in contact with Si particles, so that most Ni sheets are not transformed into nickel silicide. Lastly, $FeSi_2$-coated Si particles were synthesized via solvent evaporation process. Iron nitrate ($Fe(NO_3)_2$) aqueous solution and Si particles were mixed together and water was evaporated at 60 °C. Subsequent thermal annealing at 900 °C for 1 h in Ar/H_2 led to a formation of $FeSi_2$-coated Si particles with Fe contents of 10 wt % (Figure 2d). All metal- and/or metal silicide-coating layers were uniformly distributed on the Si surface, as evidenced by energy dispersive X-ray spectroscopy (EDS) mapping images (Supporting Information, Figure S2).

Electrochemical Test of Macroporous Si Particles with Various Coating Layers. We investigated electrochemical performances of porous Si electrodes with various coating layers with coin-type half-cells in the range of 0.005−1.2 V. Figure 3a shows the first cycle (discharging (lithiation) and charging (delithiation)) voltage profile of porous Si electrodes without any coating layers at a rate of C/20. The first discharge capacity was 2886 mAh g^{-1} with a high initial Coulombic efficiency of 90.5%. Subsequent cycle voltage profiles (2nd, 10th, 30th, 50th, and 100th) were obtained at a rate of C/5, and a specific capacity was significantly decayed at the 100th cycle, corresponding to capacity retention of 17% compared with that in the second cycle (Figure 3a). Typically, thick SEI layers were formed on the surface of bare Si without any coating layers, and subsequently, they disturbed access of lithium ions and electrolytes, leading to dramatic decay of specific capacity.[38,39]

In contrast, Si electrodes with various coating layers showed significantly improved electrochemical performances, as shown in Figure 3b−3f. Carbon-coated Si electrodes show a high initial Coulombic efficiency of 92.8% with first-cycle discharge capacity of 2820 mAh g^{-1} at a rate of C/20. Subsequent cycling performances are much better than that of bare Si electrodes, corresponding to the capacity retention of 58% after 100 cycles (Figure 3b and f). Interestingly, dramatic capacity decay of the carbon-coated Si electrodes was observed near the 80th cycle. It may be attributed to a formation of thick SEI layers, as will be discussed later. The Cu/Cu_3Si-coated Si electrode showed a high discharge capacity of 2884 mAh g^{-1} with a Coulombic efficiency of 89% at the first cycle (Figure 3c). Compared to carbon-coated Si electrodes, cycling retention of the Cu/Cu_3Si-coated Si electrode was significantly improved (capacity retention of ~65% after 100 cycles) (Figure 3f). It may be attributed to a formation of stable SEI layers, as reported in other Cu- and/or copper silicide-coated Si.[31,36]

In the case of Ni-coated Si electrode, initial Coulombic efficiency (86% at the first cycle) is slightly low, compared to other electrodes. The first-cycle voltage profile of the Ni-coated Si electrodes shows that an additional peak is observed at ~0.75 V (vs Li/Li^+). Probably small amounts of nickel oxide still remain in the Ni-coated Si particles, even after the reduction process of $Ni(OH)_2$. However, from the second cycle, the peaks corresponding to the side reaction were not seen (Figure 3d). The capacity retention of the Ni-coated Si was ~75% after 100 cycles, compared to the initial specific capacity. As another model system, iron silicide ($FeSi_2$)-coated Si shows enhanced initial Coulombic efficiency of 89.4% (Figure 3e) and capacity retention of 61% after 100 cycles, indicating that pure $FeSi_2$ layers stabilize Si-based electrodes, resulting in improvement of the electrochemical performance during cycles. Overall, Cu/Cu_3Si-, Ni-, and $FeSi_2$-coated Si electrodes showed significantly improved cycling performances compared to carbon-coated Si electrode, even though micrometer-sized Si particles were used as anode materials.

Moreover, we investigated rate capabilities of Cu/Cu_3Si-, Ni-, and $FeSi_2$-coated porous Si electrodes (Supporting Information, Figure S3). A C rate for the Li insertion was fixed at C/5, and the Li extraction rate was varied from C/5 to 10C. Cu/Cu_3Si- and $FeSi_2$-coated Si electrodes showed excellent rate capabilities (specific capacity of >1600 mAh g^{-1} at 7C), while Ni-coated Si electrode exhibited a specific capacity of ~1250 mAh g^{-1} at 7C due to weak contact of the flake-type Ni sheet with the Si surface.

To understand excellent rate capabilities of metal/metal silicide-coated Si electrodes, the electrochemical impedance spectroscopy (EIS) measurements of porous Si and Cu/Cu_3Si-, Ni-, and $FeSi_2$-coated Si electrodes were performed after 100 cycles (Supporting Information, Figure S4). Cu/Cu_3Si-coated Si electrode displayed the lowest interfacial resistance (147 ohm) including the SEI and charge transfer resistance. Ni-coated Si electrode showed high interfacial resistance (302 ohm). This is in good agreement with the EIS result that Ni-coated Si electrode exhibited inferior rate capability (Supporting Information, Figure S3).

Besides cycling performance and rate capability, the volume change of Si electrodes is a critically important issue in LIBs. Large volume changes result in significant pulverization of Si particles as a Li hosting material and a continuous SEI-filming process, which is caused by severe electrolyte decomposition on the active Si surface exposed by pulverization. This process consumes the limited Li^+ source in a cell and leads to undesirable volume expansion of Si electrodes.

Figure 4 displays cross-sectional SEM images of carbon-, Cu/Cu_3Si-, Ni-, and $FeSi_2$-coated Si electrodes before and after 100 cycles. Carbon-coated Si electrodes showed a severe volume expansion of ~500% (Figure 4a). This result suggests that amorphous carbon is not enough to alleviate a considerable volume expansion of micrometer-sized Si electrode and the formation of a thick SEI layer on the carbon and/or Si surface during a long-term cycling. In contrast, Cu/Cu_3Si-, Ni-, and $FeSi_2$-coated Si electrode showed significantly reduced volume expansion (Cu/Cu_3Si, 125%; Ni, 113%; and $FeSi_2$, 233%), compared to the carbon-coated Si electrode (Figure 4b–d). It may be attributed to the formation of a stable SEI layer on the Si surface modified with metal/metal silicide. The stable SEI layers can effectively prevent a continuous SEI-filming process during long-term cycling, resulting in reduced volume

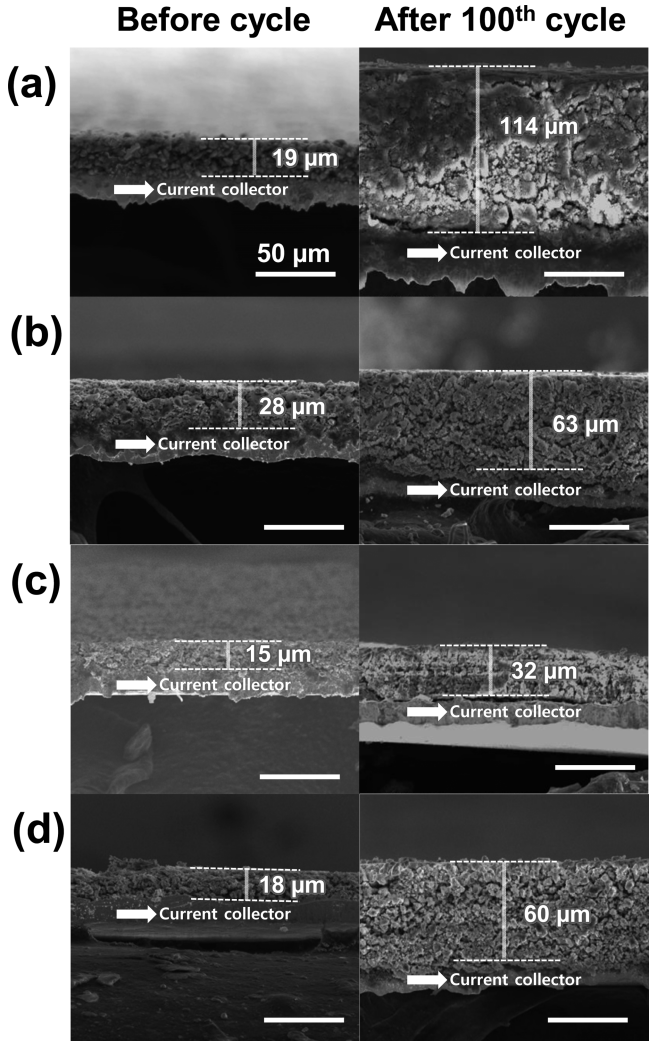

Figure 4. Cross-sectional SEM images of porous Si electrodes before and after 100 cycles: (a) carbon-coated Si, (b) Cu/Cu_3Si-coated Si, (c) Ni-coated Si, and (d) $FeSi_2$-coated Si electrodes.

expansion of metal/metal silicide-coated Si electrodes compared to carbon-coated Si electrodes.

The effects of coating materials on the surface chemistry of porous Si were confirmed by a comparison of the XPS spectra measured from electrodes after 100 cycles at room temperature. Figure 5 shows the comparison of the C 1s and F 1s spectra for the SEIs formed on porous Si electrodes coated with carbon, $Cu/CuSi_3$, Ni, and $FeSi_2$. Carbon-coated porous Si electrode showed a pronounced peak corresponding to carbon bonded to hydrogen (−C−H) at 284.8 eV when compared with the peak intensity for the C−H group and LiF in the C 1s and F 1s spectra of Figure 5a. This implies that C−H moieties are abudant in the SEI layer formed on carbon-coated porous Si electrode. The F 1s core level peaks assigned to the P−F moiety and LiF were clearly observed for all porous Si electrodes, as shown in the F 1s spectra of Figure 5.

A noticeable feature for carbon-coated porous Si electrode in the F 1s spectra is a relatively small fraction of the LiF peak at 685 eV compared with Cu/Cu_3Si-, Ni-, and $FeSi_2$-coated porous Si electrodes. This result suggests that fluoroethylene carbonate (FEC) in the electrolyte does not produce LiF as a dominant SEI constituent on carbon-coated porous Si electrode. Additionally, the F 1s spectra clearly show that the

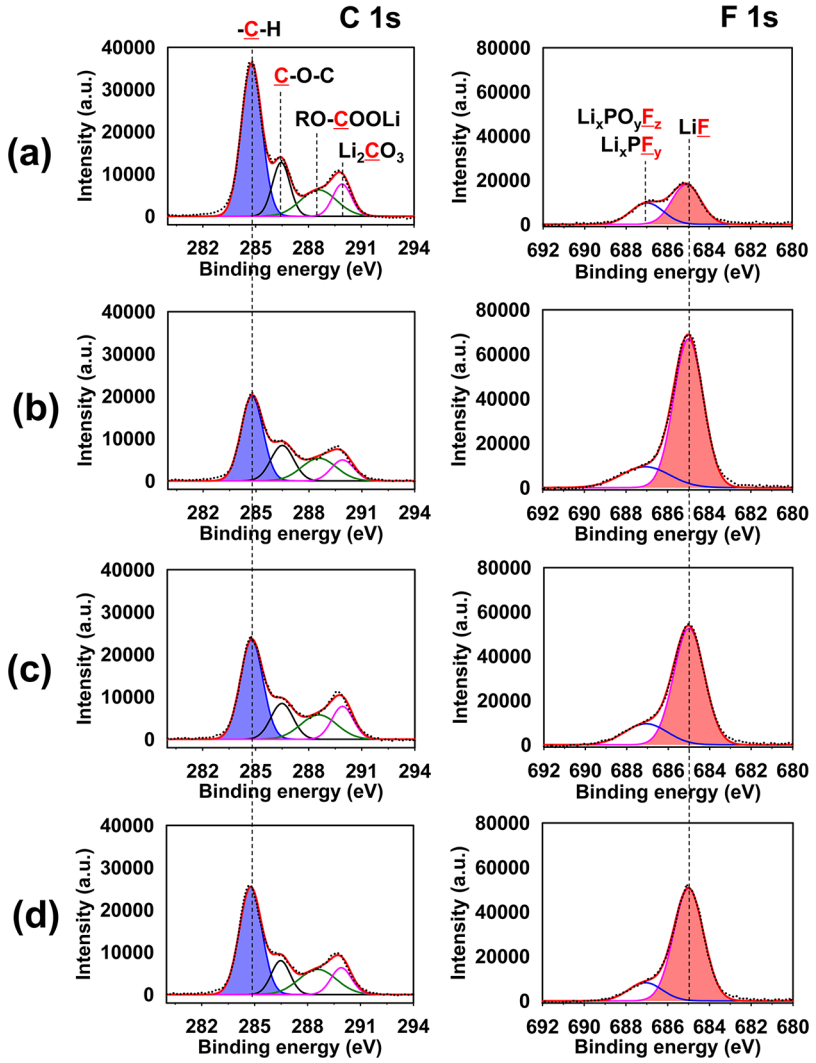

Figure 5. C 1s and F 1s XPS spectra after 100 cycles of (a) carbon-coated porous Si, (b) Cu/$CuSi_3$-coated porous Si, (c) Ni-coated porous Si, and (d) $FeSi_2$-coated porous Si electrodes.

surface film of Cu/Cu_3Si-, Ni-, and $FeSi_2$-coated porous Si electrodes contains a relatively large fraction of LiF formed by the electrochemical reduction of FEC with the relatively low lowest unoccupied molecular orbital (LUMO) energy compared to EC.[40] It is worthy to note that the LiF-based SEI is very effective to stabilize the Si−electrolyte interface.[27] From the XPS results, we could confirm that carbon-coated Si electrode has a relatively large fraction of hydrocarbon-based compounds in the SEI layer (Figure 5a), and Cu/Cu_3Si-, Ni-, and $FeSi_2$-coated porous Si electrodes lead to the formation of the LiF-based SEI layer with less hydrocarbon compounds (Figure 5b−d).

CONCLUSION

We have successfully synthesized micrometer-sized porous Si particles using Cu-assisted wet chemical etching process. To improve electrochemical performance of micrometer-sized Si particles, we introduced amorphous carbon, Cu/Cu_3Si, Ni, and $FeSi_2$ coating layers on the Si surface using a simple chemical reduction and subsequent thermal annealing process. We found that metal- and/or metal silicide-coated Si electrodes showed significantly improved electrochemical properties including a highly stable cycling performance, excellent rate capability, and a control of volume expansion. From XPS analysis, metal- and/or metal silicide-coated layers contribute to a formation of stable SEI layers on the Si surface, leading to improved electrochemical properties of micrometer-sized Si electrodes.

ASSOCIATED CONTENT

Supporting Information

Raman spectrum of carbon-coated Si, EDS mapping image of each Cu/Cu_3Si-, Ni-, and $FeSi_2$-coated porous Si particles, and EIS results of each Cu/Cu_3Si-, Ni-, and $FeSi_2$-coated porous Si electrode. This material is available free of charge via the Internet at http://pubs.acs.org.

AUTHOR INFORMATION

Corresponding Authors

*E-mail: nschoi@unist.ac.kr.
*E-mail: spark@unist.ac.kr.

Notes

The authors declare no competing financial interest.

ACKNOWLEDGMENTS

This work was supported by the IT R&D program of MOTIE/KEIT (10046309).

REFERENCES

(1) Brousse, T.; Retoux, R.; Herterich, U.; Schleich, D. M. Thin-Film Crystalline SnO2-Lithium Electrodes. *J. Electrochem. Soc.* **1998**, *145*, 1−4.

(2) Gao, X. P.; Bao, J. L.; Pan, G. L.; Zhu, H. Y.; Huang, P. X.; Wu, F.; Song, D. Y. Preparation and Electrochemical Performance of Polycrystalline and Single Crystalline CuO Nanorods as Anode Materials for Li Ion Battery. *J. Phys. Chem. B* **2004**, *108*, 5547−5551.

(3) Derrien, G.; Hassoun, J.; Panero, S.; Scrosati, B. Nanostructured Sn−C Composite as an Advanced Anode Material in High-Performance Lithium-Ion Batteries. *Adv. Mater.* **2007**, *19*, 2336−2340.

(4) Dailly, A.; Ghanbaja, J.; Willmann, P.; Billaud, D. Lithium Insertion into New Graphite−Antimony Composites. *Electrochim. Acta* **2003**, *48*, 977−984.

(5) Seo, M.-H.; Park, M.; Lee, K. T.; Kim, K.; Kim, J.; Cho, J. High Performance Ge Nanowire Anode Sheathed with Carbon for Lithium Rechargeable Batteries. *Energy Environ. Sci.* **2011**, *4*, 425−428.

(6) Yim, C.-H.; Courtel, F. M.; Abu-Lebdeh, Y. A High Capacity Silicon-Graphite Composite as Anode for Lithium-Ion Batteries Using Low Content Amorphous Silicon and Compatible Binders. *J. Mater. Chem. A* **2013**, *1*, 8234−8243.

(7) Varghese, B.; Reddy, M. V.; Yanwu, Z.; Lit, C. S.; Hoong, T. C.; Subba Rao, G. V.; Chowdari, B. V. R.; Wee, A. T. S.; Lim, C. T.; Sow, C.-H. Fabrication of NiO Nanowall Electrodes for High Performance Lithium Ion Battery. *Chem. Mater.* **2008**, *20*, 3360−3367.

(8) Park, J. H.; Hudaya, C.; Kim, A. Y.; Rhee, D. K.; Yeo, S. J.; Choi, W.; Yoo, P. J.; Lee, J. K. Al-C Hybrid Nanoclustered Anodes for Lithium Ion Batteries with High Electrical Capacity and Cyclic Stability. *Chem. Commun.* **2014**, *50*, 2837−2840.

(9) Chan, C. K.; Peng, H.; Liu, G.; Mcilwrath, K.; Zhang, X. F.; Huggins, R. A.; Cui, Y. High-Performance Lithium Battery Anodes Using Silicon Nanowires. *Nat. Nanotechnol.* **2008**, *3*, 31−35.

(10) Cui, L.-F.; Hu, L.; Wu, H.; Choi, J. W.; Cui, Y. Inorganic Glue Enabling High Performance of Silicon Particles as Lithium Ion Battery Anode. *J. Electrochem. Soc.* **2011**, *158*, A592−A596.

(11) Yu, C.; Li, X.; Ma, T.; Rong, J.; Zhang, R.; Shaffer, J.; An, Y.; Liu, Q.; Wei, B.; Jiang, H. Silicon Thin Films as Anodes for High-Performance Lithium-Ion Batteries with Effective Stress Relaxation. *Adv. Energy Mater.* **2012**, *2*, 68−73.

(12) Maranchi, J. P.; Hepp, A. F.; Kumta, P. N. High Capacity, Reversible Silicon Thin-Film Anodes for Lithium-Ion Batteries. *Electrochem. Solid-State Lett.* **2003**, *6*, A198−A201.

(13) Ulldemolins, M.; Le Cras, F.; Pecquenard, B.; Phan, V. P.; Martin, L.; Martinez, H. Investigation on the Part Played by the Solid Electrolyte Interphase on the Electrochemical Performances of the Silicon Electrode for Lithium-Ion Batteries. *J. Power Sources* **2012**, *206*, 245−252.

(14) Thakur, M.; Isaacson, M.; Sinsabaugh, S. L.; Wong, M. S.; Biswal, S. L. Gold-Coated Porous Silicon Films as Anodes for Lithium Ion Batteries. *J. Power Sources* **2012**, *205*, 426−432.

(15) Park, O.; Lee, J.-I.; Chun, M.-J.; Yeon, J.-T.; Yoo, S.; Choi, S.; Choi, N.-S.; Park, S. High-Performance Si Anodes with a Highly Conductive and Thermally Stable Titanium Silicide Coating Layer. *RSC Adv.* **2013**, *3*, 2538−2542.

(16) Lin, Y.-M.; Klavetter, K. C.; Abel, P. R.; Davy, N. C.; Snider, J. L.; Heller, A.; Mullins, C. B. High Performance Silicon Nanoparticle Anode in Fluoroethylene Carbonate-Based Electrolyte for Li-Ion Batteries. *Chem. Commun.* **2012**, *48*, 7268−7270.

(17) Ru, Y.; Evans, D. G.; Zhu, H.; Yang, W. Facile Fabrication of Yolk-Shell Structured Porous Si-C Microspheres as Effective Anode Materials for Li-Ion Batteries. *RSC Adv.* **2014**, *4*, 71−75.

(18) Liu, N.; Lu, Z.; Zhao, J.; Mcdowell, M. T.; Lee, H.-W.; Zhao, W.; Cui, Y. A Pomegranate-Inspired Nanoscale Design for Large-Volume-Change Lithium Battery Anodes. *Nat. Nanotechnol.* **2014**, *9*, 187−192.

(19) Chen, S.; Gordin, M. L.; Yi, R.; Howlett, G.; Sohn, H.; Wang, D. Silicon Core-Hollow Carbon Shell Nanocomposites with Tunable Buffer Voids for High Capacity Anodes of Lithium-Ion Batteries. *Phys. Chem. Chem. Phys.* **2012**, *14*, 12741−12745.

(20) Bang, B. M.; Kim, H.; Lee, J.-P.; Cho, J.; Park, S. Mass Production of Uniform-Sized Nanoporous Silicon Nanowire Anodes Viablock Copolymer Lithography. *Energy Environ. Sci.* **2011**, *4*, 3395−3399.

(21) Wu, H.; Chan, G.; Choi, J. W.; Ryu, I.; Yao, Y.; Mcdowell, M. T.; Lee, S. W.; Jackson, A.; Yang, Y.; Hu, L.; Cui, Y. Stable Cycling of Double-Walled Silicon Nanotube Battery Anodes through Solid-Electrolyte Interphase Control. *Nat. Nanotechnol.* **2012**, *7*, 310−315.

(22) Wen, Z.; Lu, G.; Mao, S.; Kim, H.; Cui, S.; Yu, K.; Huang, X.; Hurley, P. T.; Mao, O.; Chen, J. Silicon Nanotube Anode for Lithium-Ion Batteries. *Electrochem. Commun.* **2013**, *29*, 67−70.

(23) Ye, J. C.; An, Y. H.; Heo, T. W.; Biener, M. M.; Nikolic, R. J.; Tang, M.; Jiang, H.; Wang, Y. M. Enhanced Lithiation and Fracture Behavior of Silicon Mesoscale Pillars Via Atomic Layer Coatings and Geometry Design. *J. Power Sources* **2014**, *248*, 447−456.

(24) Ma, R.; Liu, Y.; He, Y.; Gao, M.; Pan, H. Chemical Preinsertion of Lithium: An Approach to Improve the Intrinsic Capacity Retention of Bulk Si Anodes for Li-Ion Batteries. *J. Phys. Chem. Lett.* **2012**, *3*, 3555−3558.

(25) Thakur, M.; Pernites, R. B.; Nitta, N.; Isaacson, M.; Sinsabaugh, S. L.; Wong, M. S.; Biswal, S. L. Freestanding Macroporous Silicon and Pyrolyzed Polyacrylonitrile as a Composite Anode for Lithium Ion Batteries. *Chem. Mater.* **2012**, *24*, 2998−3003.

(26) Bang, B. M.; Lee, J.-I.; Kim, H.; Cho, J.; Park, S. High-Performance Macroporous Bulk Silicon Anodes Synthesized by Template-Free Chemical Etching. *Adv. Energy. Mater.* **2012**, *2*, 878−883.

(27) Chun, M.-J.; Park, H.; Park, S.; Choi, N.-S. Bicontinuous Structured Silicon Anode Exhibiting Stable Cycling Performance at Elevated Temperature. *RSC Adv.* **2013**, *3*, 21320−21325.

(28) Guo, J.; Sun, A.; Chen, X.; Wang, C.; Manivannan, A. Cyclability Study of Silicon−Carbon Composite Anodes for Lithium-Ion Batteries Using Electrochemical Impedance Spectroscopy. *Electrochim. Acta* **2011**, *56*, 3981−3987.

(29) Lee, J. K.; Yoon, W. Y.; Kim, B. K. Electrochemical Behaviors of Diamond-Like-Carbon-Coated Silicon Monoxide−Graphite Composite Anode for Li-Ion Battery. *J. Electrochem. Soc.* **2013**, *160*, A1348−A1352.

(30) Woo, S.-H.; Park, J.-H.; Hwang, S. W.; Whang, D. Silicon Embedded Nanoporous Carbon Composite for the Anode of Li Ion Batteries. *J. Electrochem. Soc.* **2012**, *159*, A1273−A1277.

(31) Murugesan, S.; Harris, J. T.; Korgel, B. A.; Stevenson, K. J. Copper-Coated Amorphous Silicon Particles as an Anode Material for Lithium-Ion Batteries. *Chem. Mater.* **2012**, *24*, 1306−1315.

(32) Wang, F.; Xu, S.; Zhu, S.; Peng, H.; Huang, R.; Wang, L.; Xie, X.; Chu, P. K. Ni-Coated Si Microchannel Plate Electrodes in Three-Dimensional Lithium-Ion Battery Anodes. *Electrochim. Acta* **2013**, *87*, 250−255.

(33) Sun, F.; Huang, K.; Liu, Y.; Gao, T.; Han, Y.; Zhong, J. Hierarchical Structure of Co3O4 Nanoparticles on Si Nanowires Array Films for Lithium-Ion Battery Applications. *Appl. Surf. Sci.* **2013**, *266*, 300−305.

(34) Yao, Y.; Liu, N.; Mcdowell, M. T.; Pasta, M.; Cui, Y. Improving the Cycling Stability of Silicon Nanowire Anodes with Conducting Polymer Coatings. *Energy Environ. Sci.* **2012**, *5*, 7927−7930.

(35) Yoo, S.; Lee, J.-I.; Ko, S.; Park, S. Highly Dispersive and Electrically Conductive Silver-Coated Si Anodes Synthesized Via a Simple Chemical Reduction Process. *Nano Energy* **2013**, *2*, 1271−1278.

(36) Kim, I.-C.; Byun, D.; Lee, S.; Lee, J. K. Electrochemical Characteristics of Copper Silicide-Coated Graphite as an Anode Material of Lithium Secondary Batteries. *Electrochim. Acta* **2006**, *52*, 1532−1537.

(37) Foggiato, J.; Yoo, W. S.; Ouaknine, M.; Murakami, T.; Fukada, T. Optimizing the Formation of Nickel Silicide. *Mater. Sci. Eng., B* **2004**, *114*−*115*, 56−60.

(38) Pereira-Nabais, C.; Świątowska, J.; Chagnes, A.; Ozanam, F.; Gohier, A.; Tran-Van, P.; Cojocaru, C.-S.; Cassir, M.; Marcus, P.

Interphase Chemistry of Si Electrodes Used as Anodes in Li-Ion Batteries. *Appl. Surf. Sci.* **2013**, *266*, 5−16.
(39) Oumellal, Y.; Delpuech, N.; Mazouzi, D.; Dupre, N.; Gaubicher, J.; Moreau, P.; Soudan, P.; Lestriez, B.; Guyomard, D. The Failure Mechanism of Nano-Sized Si-Based Negative Electrodes for Lithium Ion Batteries. *J. Mater. Chem.* **2011**, *21*, 6201−6208.
(40) Song, Y. M.; Han, J. G.; Park, S.; Lee, K. T.; Choi, N. S. A Multifunctional Phosphite-Containing Electrolyte for 5 V-Class $LiNi_{0.5}Mn_{1.5}O_4$ Cathodes with Superior Electrochemical Performance. *J. Mater. Chem. A* **2014**, *2*, 9506−9513.